CROATICA CHEMICA ACTA CCACAA 48 (4) 521—538 (1976)

CCA-956

YU ISSN 0011-1643
541.18
Conference Paper

Characterization of the Surface of High-Area $Ni(OH)_2$ and NiO

C. Cronan, F. J. Micale, H. Leidheiser, Jr., M. Topić, and A. C. Zettlemoyer*

Center for Surface and Coatings Research Lehigh University, Bethlehem, Pennsylvania, USA

The surface properties of $Ni(OH)_2$, and the mechanism of decomposition of $Ni(OH)_2$ to NiO were investigated by a variety of experimental approaches including gas adsorption, heats of immersion and diffuse ir reflectance. The $Ni(OH)_2$ samples were prepared by bubbling ammonia gas through a $Ni(NO_3)_2$ solution at different temperatures. $Ni(OH)_2$ is relatively hydrophobic while NiO is completely hydrophilic. A relationship was established between the specific surface areas of the parent $Ni(OH)_2$ and its decomposition product NiO which supports a mechanism of dehydration at 200 °C involving separation along the hexagonal planes. This mechanism was confirmed by electron micrographs during decomposition of $Ni(OH)_2$ to NiO.

Gravimetric studies of the decomposition of $Ni(OH)_2$ at 200 °C indicated that approximately 14% of the hydroxyl groups are not removed. Diffuse ir reflectance studies showed that surface hydroxyls were not removed. Physical adsorption of water vapor on $Ni(OH)_2$ as a function of surface area supports the hypothesis that the basal planes are hydrophobic and the crystal edges are hydrophilic.

INTRODUCTION

The catalytic[1] and electrical[2] properties of NiO are well known and fill many pages of the literature. The importance of NiO as a subject of investigation lies in the surface properties which render this material useful as an industrial catalyst in many different types of oxidation reactions. Although the surface investigation of single crystals of NiO may be considered more fruitful from a theoretical point of view, the investigation of heterogenous high surface area powders is more practical in that the high area materials relate more closely to real industrial catalysts. High surface area NiO can be prepared by the dehydration at elevated temperatures of precipitated $Ni(OH)_2$. Very little work has been reported in the literature[3] on the surface properties of $Ni(OH)_2$, and no work has been directed towards a correlation between the surface properties of NiO and its precursor $Ni(OH)_2$.

This paper represents a summary of results on the surface properties of $Ni(OH)_2$, NiO, and the mechanism of transition of $Ni(OH)_2$ to NiO. The tools of investigation include gas adsorption, both argon and water vapor, heats of immersion in water, x-ray analysis, and electron microscopy. The ultimate objective of this investigation is to relate the intensive and extensive surface properties of $Ni(OH)_2$ that may be altered by different sample precipitation conditions, to the surface properties of NiO.

* Current address — »Ruđer Bošković« Institute, 41000 Zagreb, Croatia, Yugoslavia

The preparation of oxides by the thermal decomposition of metal hydroxides has wide usefulness. For example, the thermal decomposition of $Mg(OH)_2$ to MgO is a procedure in oxide ceramics. During studies concerned with the surface characterization of $Ni(OH)_2$ and NiO, surface area changes that occurred during thermal decomposition have led to some rather interesting insights concerning the mechanism of decomposition. A literature review of similar hydroxides, furthermore, has suggested that this mechanism may not be unique to $Ni(OH)_2$. Therefore, a mechanism of thermal decomposition will be proposed herein for $Ni(OH)_2$ that may be generally applicable to systems with the same crystallographic relationship between reactant and product.

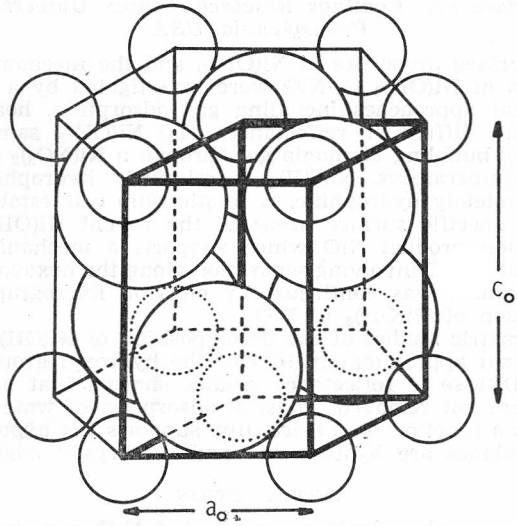

Figure 1. The $Ni(OH)_2$ crystal structure (CdI_2 type) with emphasis of the hexagonal unit cell. Small spheres are nickel ions, large spheres are oxygen. Hydrogen atoms are not indicated.

Nickel hydroxide has the brucite (also designated as CdI_2 or PbI_2) structure which can best be described as a hexagonal layered structure[4]. Figure 1 provides an illustration of this type structure which is shared by other metal hydroxides such as $Mg(OH)_2$ (brucite), $Ca(OH)_2$ (portlandite), $Mn(OH)_2$, $Fe(OH)_2$, $Co(OH)_2$, and $Cd(OH)_2$. These compounds can be converted by thermal decomposition to an oxide with the cubic rock salt structure.

$$M(OH)_2 \rightarrow MO + H_2O\uparrow$$
brucite rock salt

The possible mechanism of such a transformation for these and similar materials have been reviewed by Brett, *et al.*[5].

Considerable topotaxy has been observed in the process of decomposition of $Mg(OH)_2$[6,7] and $Ni(OH)_2$[8] to the oxides. For example, the basal hexagonal plane (0001) of the hydroxide becomes the hexagonally packed (111) plane of the cubic oxide. The conclusion of most authors has been that the hexagonally shaped particles of oxide contain tiny cubic-shaped crystallites, with dimensions of less than 7nm, which are somehow bound together within the

general shape of the hexagonal parent hydroxide crystal. This conclusion is based on observed properties such as x-ray line broadening, magnetic measurements, and the increase in surface area upon decomposition. The purpose of this communication is to propose an alternative explanation for these observed properties of the oxides as prepared by thermal decomposition of the parent hexagonally layered hydroxides.

THEORY

The specific surface area, Σ, of a material which consists totally of identical regular hexagonal plates may be expressed by the following equation:

$$\Sigma = \frac{2R + CH}{RH\varrho} \tag{1}$$

$$C = \frac{4\sqrt{3}}{3} = 2.309$$

where R = radius or edge of the hexagonal plates
H = thickness of the hexagonal plates
ϱ = sample density
C = is a factor derived from the geometry of the hexagonal plate

The following derivation requires two assumptions: the $M(OH)_2$ consists of monodisperse hexagonal plates, each of radius R_1 and height H_1, and each $M(OH)_2$ hexagonal plate splits into n identical layers of MO, each layer being a hexagonal plate of radius R_2 and height H_2. This process is shown schematically in Figure 2. The physical properties of $Ni(OH)_2$ and NiO, Table I, show

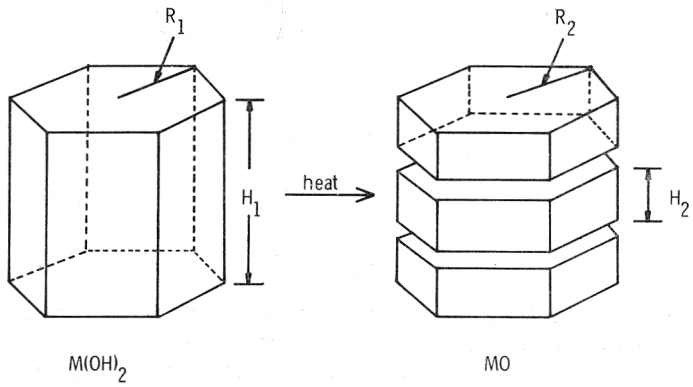

Figure 2. Schematic diagram of the splitting of the hydroxide plate, of »radius« R_1 and thickness H_1, into several thinner plates of oxide, of »radius« R_2 and thickness H_2, upon thermal decomposition in vacuum.

that there is a 53% (54% for $Mg(OH)_2$) decrease in the molar volume during thermal decomposition. This diminution in volume indicates that the dimensions of the NiO plates must be smaller than the respective dimensions of $Ni(OH)_2$. Two parameters can be introduced to account for these dimensional changes. These parameters, which can be calculated from available x-ray data, will be designated r and h, such that:

TABLE I

Some Physical Properties of the $Ni(OH)_2/NiO$ and $Mg(OH)_2/MgO$ Systems

	$Ni(OH)_2$	NiO	$Mg(OH)_2$	MgO
Molecular Weight (g)	92.71	74.69	58.34	40.32
X-ray Density (g/cm^3)	3.950	6.809	2.370	3.580
Molar Volume (cm^3/mol)	23.47	10.97	24.62	11.26

$$nH_2 = hH_1 \tag{2}$$

$$R_2 = rR_1 \tag{3}$$

where the subscripts 1 and 2 refer to $M(OH)_2$ and MO, respectively, the specific surface area of $M(OH)_2$ and MO may be expressed by the equations:

$$\Sigma_1 = \frac{2R_1 + CH_1}{R_1H_1\varrho_1} = \frac{2R_1 + \frac{Cn}{h}H_2}{R_1\frac{n}{h}H_2\varrho_1} \tag{4}$$

and

$$\Sigma_2 = \frac{2R_2 + CH_2}{R_2H_2\varrho_2} = \frac{2rR_1 + CH_2}{rR_1H_2\varrho_2} \tag{5}$$

Equations (4) and (5) may be combined through the elimination of R_1.

$$\Sigma_2 = \frac{\varrho_1}{r\varrho_2}\Sigma_1 + \frac{2}{H_2\varrho_2}\left(1 - \frac{h}{rn}\right) \tag{6}$$

and rearranged:

$$\frac{\Sigma_2}{\Sigma_1} = \frac{2}{H_2\varrho_2}\left(1 - \frac{h}{rn}\right)\frac{1}{\Sigma_1} + \frac{\varrho_1}{r\varrho_2} \tag{7}$$

Equation (7) predicts that Σ_2/Σ_1, is a linear function of $1/\Sigma_1$ only if

$$\text{Slope} = \frac{2}{H_2\varrho_2}\left(1 - \frac{h}{rn}\right) \tag{8}$$

is constant. The terms H_2 and n, however, are functions of both Σ_1 and Σ_2. In actual practice H_2 will be shown not to vary significantly for the relatively high surface area samples investigated. The net result appears to be that the slope in Equation (7) remains effectively constant.

The constants r and h can be evaluated through the use of available x-ray data[9] as tabulated in Table II. The hexagonal (0001) plane of the $M(OH)_2$ structure can be directly compared to the (111) plane of the face centered cubic MO structure.

The distance between (0001) nickel planes in the hydroxide is the parameter c_o; the corresponding distance in NiO is that between (111) planes, d_{111}. Thus the contraction in the thickness of the hexagonal plate upon thermal decomposition is

TABLE II

X-ray Data of the Hydroxides[17] and Oxides of Nickel and Magnesium

	$Ni(OH)_2$	$Mg(OH)_2$
c_o [nm]	0.4605	0.4769
a_o [nm]	0.3126	0.3147

	NiO	MgO
a [nm]	0.41769	0.4213
d_{111} [nm]	0.2410	0.2431
d_{220} [nm]	0.1476	0.1489

$$h = \frac{d_{111}}{c_0} = 0.5233 \text{ for } Ni(OH)_2. \tag{8a}$$

Similarly the M-M distance in the (0001) plane of the hydroxide is the parameter a_o; the corresponding distance in the (111) plane of the oxide is $d_{110} = 2d_{220}$. The contraction in the edge or radius of the hexagonal face upon thermal decomposition is then

$$r = \frac{2d_{220}}{a_0} = 0.9443 \text{ for } Ni(OH)_2. \tag{8b}$$

The corresponding values of h and r for $Mg(OH)_2$ are 0.5098 and 0.9463, respectively.

The foregoing considerations suggest that a plot of Σ_2/Σ_1 *vs.* $1/\Sigma_1$ for various samples of NiO produced from the thermal decomposition of $Ni(OH)_2$ should be linear with

$$\text{Intercept} = \frac{\varrho_1}{r\varrho_2} = 0.614. \tag{9}$$

From Equation (8):

$$\text{Slope} = \frac{293.7}{H_2}\left(1 - \frac{0.5542}{n}\right). \tag{10}$$

For $Mg(OH)_2$, the intercept should be 0.700 and

$$\text{Slope} = \frac{558.7}{H_2}\left(1 - \frac{0.5387}{n}\right). \tag{11}$$

In both Equations (10 and (11) the slope is in units of m^2/g if H_2 is in nm.

EXPERIMENTAL

The results presented in this paper were obtained on $Ni(OH)_2$ samples prepared by various techniques, and are designated A through F. Samples A and C were prepared by bubbling ammonia gas through nickel nitrate solutions of concentration 0.45 M at 35 °C and 25 °C, respectively. Sample B was similarly prepared from a 0.086 M solution of nickel nitrate at 25 °C. The precipitates were washed with deionized water and centrifuged until the wash water attained a constant conductivity of 3.3×10^{-6} ohm^{-1} cm^{-1}. Samples D, E, and F were obtained from Dr. Velimir Pravdić (»Ruđer Bošković« Institute, Zagreb, Croatia, Yugoslavia). Samples D and E were prepared by a modified sol-gel process[10]. Sample F was prepared by precipitation

from a nickel chloride solution with sodium hydroxide. Purification for all three samples was achieved by a dialysis technique. The decomposition of $Ni(OH)_2$ to NiO was performed in high vacuum at 200 °C for samples A through E, and at 250 °C for sample F. The literature values for the specific surface areas of $Ni(OH)_2$ and NiO, samples 1 through 6, were obtained on samples precipitated from $Ni(NH_3)_x^{++}$ complex by distilling off excess NH_3, washing, and then thermally decomposing to the oxide at 200 °C in high vacuum. The basic difference in preparation between samples A through F and the literature samples is that samples A through F were precipitated by adding ammonia or sodium hydroxide, whereas the literature samples were precipitated by removing excess ammonia.

Nitrogen and/or argon gas adsorption isotherms for specific surface area determination were obtained at liquid nitrogen temperature using a classical BET volumetric vacuum rig. The residual pressure of 10^{-6} torr was monitored by an ion gauge. A capacitive electronic manometer equipped with a 1000 torr (133.322 kPa) differential pressure transducer (Datametrics, Inc.) was used to measure the gas pressure with a sensitivity of 10^{-3} torr. Specific surface areas were calculated for nitrogen and argon molecular crosssections of 0.162 nm^2 and 0.166 nm^2, respectively. Surface areas reported in this paper were obtained with a prepurified research grade argon gas from J. T. Baker Chemical Co.

The heats of immersion in water were measured in a thermistor type adiabatic calorimeter[7]. The temperature changes in the calorimeter vessel were followed by measuring the change in resistance of the thermistor in a Wheatstone bridge and reccording the off balance of the bridge after amplification by a Hewlett-Packard DC Null Voltmeter 419A. The workable sensitivity was 1×10^{-4} °C with a background noise of 2×10^{-4} °C. The sources of error in this calorimeter, *i. e.* instrument sensitivity, reproducibility of heat of bulb breaking and reproducibility of heat capacity determination, led to a cumulative error of ± 0.13 J for each heat of immersion measurement[7]. The average experimental uncertainty for the heat of immersion of $Ni(OH)_2$ in water was estimated at ± 15 mJ/m^2.

The water adsorption isotherms were measured on a quartz spring (Worden Quartz Co.) with a sensitivity of 10 μg per gram of sample or 0.02 molecules of water adsorbed per nm^2. The equilibrium pressure was measured with a 100 torr (13332 Pa) capacitive differential manometer (Datametrics Inc.) which had a sensitivity of 2×10^{-4} torr. The water isotherm temperatures, determined at 25° and 39 °C, were controlled to within ± 0.5 °C. The activation conditions of samples for all isotherms was 39 °C at 10^{-6} torr for 16 hours. The isotherms were reversible at the temperatures investigated.

RESULTS AND DISCUSSION

Sample Size and Shape

A typical electron micrograph of sample B is presented in Figure 3. Analysis of several micrographs show that the $Ni(OH)_2$ particles consists of hexa-

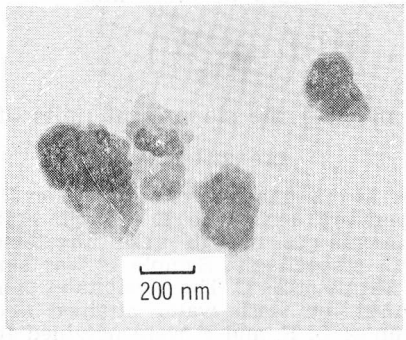

Figure 3. Electron micrograph of $Ni(OH)_2$, sample B, illustrating the approximately hexagonally shaped platelets.

gonal platelets which vary in size from 40 nm to 400 nm. Pt shadowing techniques indicated platelet thicknesses varying from 13 nm to approximately 50 nm. No essential differences in particle size and shape were observed for sample A. Sample A was also analyzed by x-ray diffraction using Cu—$\varkappa\alpha$ radiation and a counter diffractometer in order to determine crystallite size and relative crystal lattice distortion. A portion of the x-ray diffraction pattern for $Ni(OH)_2$ is shown in Figure 4. The sharp diffraction pattern

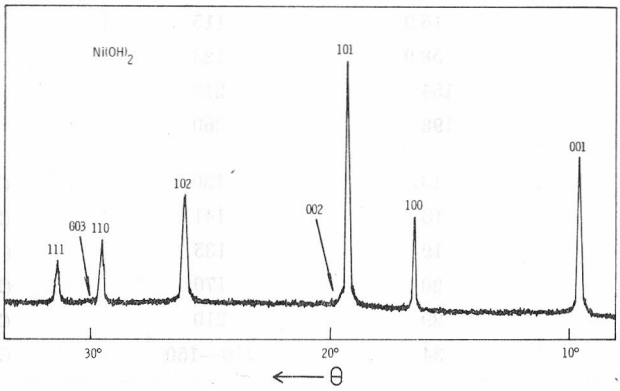

Figure 4. A portion of the x-ray diffraction pattern for $Ni(OH)_2$. The ordinate is intensity. The reflections are indexed as shown.

exhibited by the hexagonal $Ni(OH)_2$ (unit cell: $a_o = 0.312$ nm, $C_o = 0.460$ nm, space group $P\bar{3}$ m1, density = 3.95 g/cm³) does not contain convenient higher orders of refraction from the same crystal planes, and the separation of dispersion and distortion broadening was not made. Assuming that all diffraction broadening was dispersion broadening, the crystallite size of $Ni(OH)_2$ was estimated to be larger than 100 nm.

Attempts were made to observe the splitting of hexagonal plates during the thermal decomposition of $Ni(OH)_2$ to NiO. Electron micrographs were taken of NiO (sample A, Table III) produced above 200 °C on the hot stage of a Phillips 300 electron microscope. Figures 5 and 6 show NiO plates which have fanned out and slipped respectively. Photographs such as these were the first confirming evidence for the possibility of a »splitting hexagonal plate« theory. The slipped plates were most plentiful if prepared out of the electron beam because the beam itself increased the temperature to some value above 200 °C. It might be noted here that such splitting was suggested by Zettlemoyer and Walker[11] who studied the surface structure of commercial active magnesia samples (MgO) prepared from $Mg(OH)_2$ in air.

NiO was analyzed by x-ray diffraction using a counter diffractometer in order to determine crystallite size and relative crystal lattice distortion. The x-ray diffraction powder pattern, Figure 7, showed well defined but very broad reflections interpreted in terms of cubic symmetry (Fm 3m, ASTM 4-0835) with unit cell dimension $a_o = 0.418$ nm. The results indicate that large NiO platelets are built up of a number of small, slightly disoriented (say 1°) crystallites. This result is in agreement with MgO results of Guilliatt and Brett[12].

TABLE III

Specific Surface Area of $Ni(OH)_2$ and NiO Samples

Sample Identification	$Ni(OH)_2$ Σ_1 [m^2/g]	NiO Σ_2 [m^2/g]	Reference
A	17.4	134	
B	33.2	125	
C	16.9	115	
D	58.9	123	
E	154	213	
F	198	260	
1	13	130	(14)
2	18	141	(22)
3	19	135	(8)
4	20	170	(23)
5	89	210	(24)
6	34	110—150	(25)

Evidence against the presence of an array of disoriented crystallites is shown in Figure 8, which is a selected area diffraction (SAD) pattern of a NiO plate. The spot pattern indicates a single crystalline plate or may indicate a single plate built up of highly oriented crystallites. Such aggregates of crystallites (as a substructure of the NiO plates) serve as an explanation that

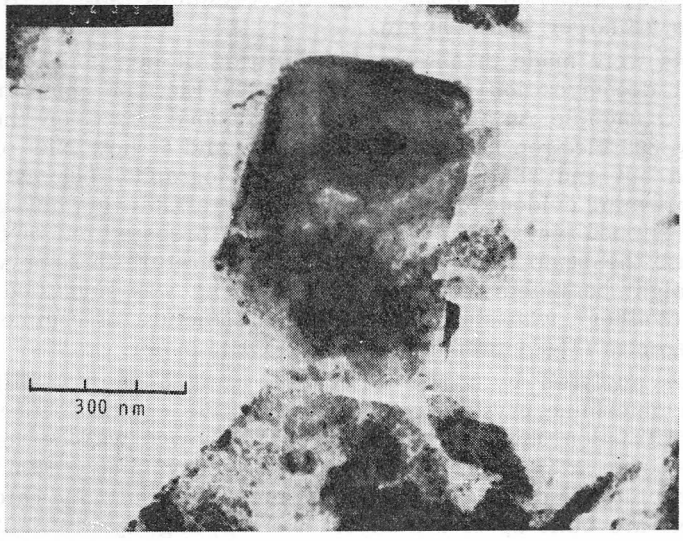

Figure 5. Electron micrograph illustrating layers of NiO which have fanned out, produced by thermal decomposition within the electron microscope.

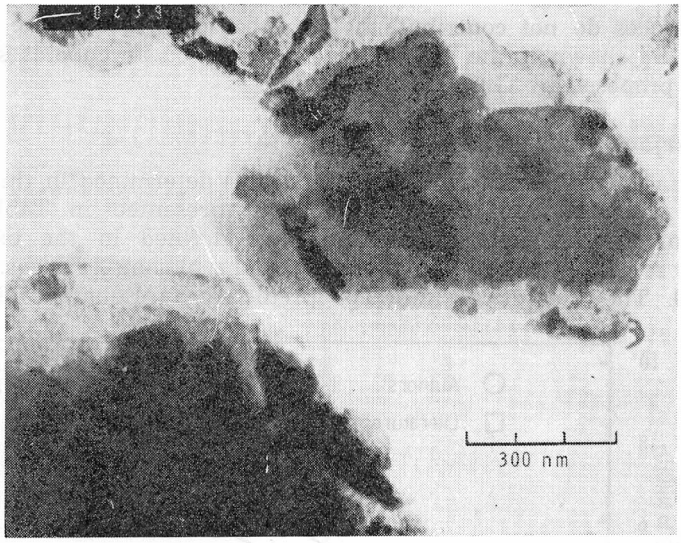

Figure 6. Electron micrograph illustrating layers of NiO which have slipped, produced by thermal decomposition within the electron microscope.

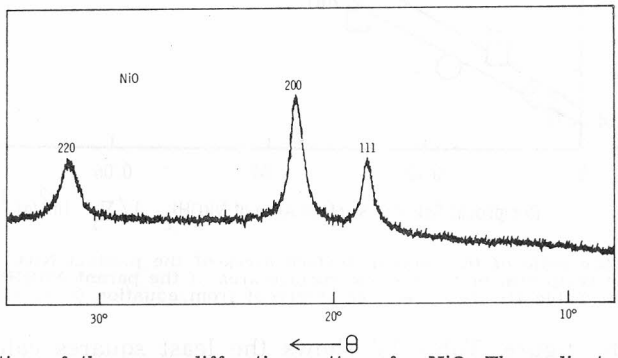

Figure 7. A portion of the x-ray diffraction pattern for NiO. The ordinate is intensity. The reflections are indexed as shown.

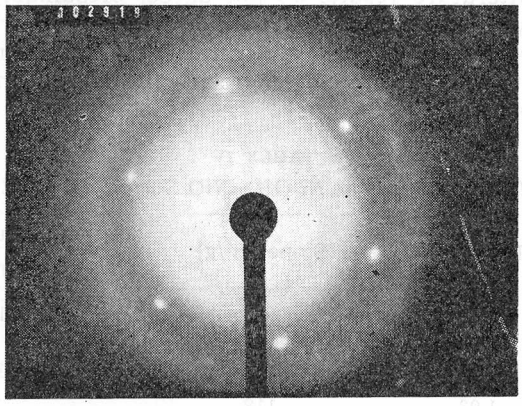

Figure 8. Selected area diffraction pattern of a NiO plate, alligned in [111] direction.

all their surfaces do not contribute to the specific surface of the plate. This concept can be shown if the crystallites are pictured as cuboids standing on a corner as proposed by Guilliatt and Brett[13].

Specific Surface Area

The surface area results on $Ni(OH)_2$ and NiO determined in this work and the results obtained from the literature are presented in Table III. The conditions of sample preparation have been defined in the experimental section. The results in Table III were used in the plot of Σ_2/Σ_1, *vs.* $1/\Sigma_1$ given in Figure 9. The theoretical intercept predicted by Equation (9), 0.614, is

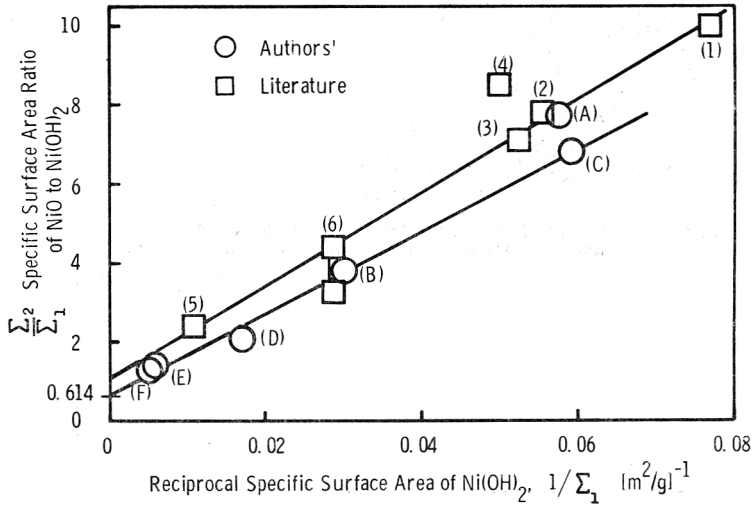

Figure 9. Plot of the ratio of the specific surface areas of the product NiO, Σ_2, to the parent $Ni(OH)_2$, Σ_1, *vs.* the reciprocal of the specific surface area of the parent $Ni(OH)_2$). Data obtained from Table III. The predicted intercept from equation (9) is 0.614.

indicated in the figure. Table IV shows the least squares calculated slopes and intercepts (neglecting literature data point #4 and sample A). Although the authors' and literature results do not agree, presumably because of different preparatory conditions of $Ni(OH)_2$, each set appears to be well represented by a straight line. The k value in Table IV is the ratio of the extrapolated intercept to the theoretical intercept, the significance of which will be discussed below.

TABLE IV

Slopes and Intercepts for the $Ni(OH)_2$/NiO Systems Plotted in Figure 3

	Intercept	Slope [m^2/g]	$k = \frac{\text{Measured Intercept}}{\text{Theoretical Intercept}}$
Theory Eqn. (9)	0.614	—	1.000
Authors'	0.637	103	1.04
Literature	1.03	118	1.68

TABLE V

Specific Surface Area of $Mg(OH)_2$ and MgO Literature Samples

Sample Identification	$Mg(OH)_2$ Σ_1 [m^2/g]	MgO Σ_2 [m^2/g]	Reference
7	30	210	(17)
8	55	240	(26)
9	89	310	(27)

TABLE VI

Slope and Intercept for the $Mg(OH)_2$/MgO System Plotted in Figure 4

	Intercept	Slope [m^2/g]	$k = \frac{\text{Measured Intercept}}{\text{Theoretical Intercept}}$
Theory Eqn. (9)	0.700	—	1.000
Literature	1.57	162	2.24

The specific surface area relationship for the $Mg(OH)_2$/MgO system may be presented in a similar manner. Table V lists $Mg(OH)_2$ and MgO surface area results with their literature references. Published data are limited for hydroxides prepared under identical conditions or thermally decomposed by a standard technique. As in the $Ni(OH)_2$/NiO case the data of Table V are restricted to precipitated $Mg(OH)_2$ thermally decomposed in vacuum at 350—400 °C. Figure 10 is a plot of these data in the form suggested by Equation (7). Table VI lists the least squares intercept and slope and the intercept calculated by Equation (9). Again k is the ratio of the literature extrapolated intercept to the theoretical intercept.

Figures 9 and 10 show some interesting characteristics. First, it is notable that the specific surface area data can be well represented with a linear plot of Σ_2/Σ_1 *vs* $1/\Sigma_1$. Second, the plot in Figure 9 indicates that the authors' and

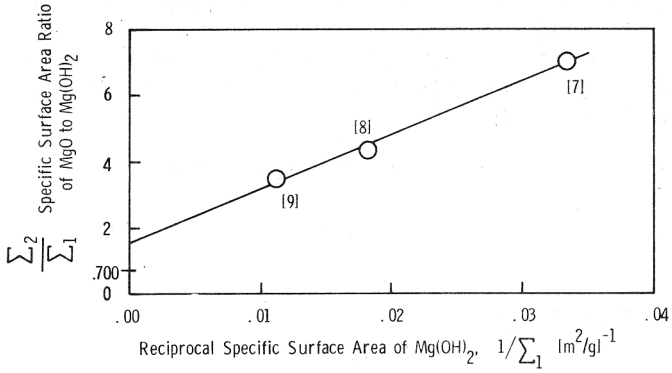

Figure 10. Plot of the ratio of the specific surface areas of the product MgO, Σ_2, to the parent $Mg(OH)_2$, Σ_1, *vs.* the reciprocal of the specific surface area of the parent $Mg(OH)_2$. Data obtained from Table V. The predicted intercept from Equation (9) is 0.700.

the literature results are not quite colinear for the nickel system. The literature results are represented by a higher slope and a higher intercept. Third, the experimental intercepts for both the nickel and magnesium systems are higher than the values predicted by Equation (9). The failure to extrapolate to the predicted intercept and the difference in the two sets of results for the $Ni(OH)_2/NiO$ system may be explained by examining the derivation of Equation (7). This equation is derived for ideal hexagonal plates with perfect crystal structure and smooth faces splitting into similarly perfect crystalline hexagonal plates. As noted earlier, the actual shape of the plate is unimportant as its effect (parameter C) is eliminated from Equation (7). Although geometrical effects may be neglected, surface and bulk irregularities as well as fracturing of the thin plates cannot. Furthermore, differences in polydispersity of the samples with respect to H_1 will cause scatter when plotted as in Figures 9 and 10. If all samples are equally polydispersed, the effect would cause a change in the slope of Equation (7).

The imperfect fit of Equatiton (7) may be due, at least in part, to bulk irregularities. The decomposition of $Ni(OH)_2$ at 200 °C actually yields a product which can be expressed as $NiO \cdot xH_2O$. The decomposition product has previously been found to have $x = 0.16$ [14] and $x = 0.18$ [15]. Gravimetric studies in this work on samples A, B, and C have found values for x of 0.13, 0.15, and 0.14, respectively, for the 200 °C decomposition, comparing well with the results cited above. In addition, new infrared reflectance studies in this laboratory have indicated that residual hydroxyls remain on the surface of the NiO product. Thermal decomposition of $Mg(OH)_2$ also has been observed[16,17] to be complete at approximately 90% of theoretical water loss at the moderate temperatures of 300 to 400 °C in vacuum. Further evidence for bulk irregularities, at least in NiO, is that its density has been measured as 6.0 g/cm^3 [8,18]. This value for NiO density would result in an intercept ratio, k, of 1.12 as compared to 1.04 for the authors' data plotted in Figure 9.

Guilliatt and Brett[12] studied, by x-ray line broadening, a series of precipitated $Mg(OH)_2$ samples. They compared the plate thickness in the [0001] direction, of the hydroxide with the [200] direction crystal thickness of the resulting oxide. They concluded that the oxide consisted of aggregates of almost octahedraly shaped MgO crystallites bound together in the same shape as the parent $Mg(OH)_2$ crystal, with the (111) planes nearly parallel to the (0001) hydroxide basal plane. However, the thickness of the oxide plate H_2, which is measured in the (111) direction, is a factor of $\sqrt{3}$ smaller than the [200] dimension thickness, calculated by Guilliatt and Brett. Substituting Equation (2) into Equation (8), we find:

$$S = \text{slope} = \frac{2}{H_2\varrho_2}\left(1 - \frac{H_2}{rH_1}\right) \tag{12}$$

or

$$H_2 = \frac{2H_1}{S\varrho_2 H_1 + \frac{2}{r}} \tag{13}$$

For precipitated $Mg(OH)_2$:

$$S = 162 m^2/g$$

$$\varrho_2 = 3.58 \text{ g/cm}^3$$

$$r = 0.9436$$

Equation (13) provides a relationship between the plate thickness of the oxide and that of the parent hydroxide, and is plotted as a function of H_1 in Figure 11. The results of Guilliatt and Brett, for precipitated $Mg(OH)_2$, are

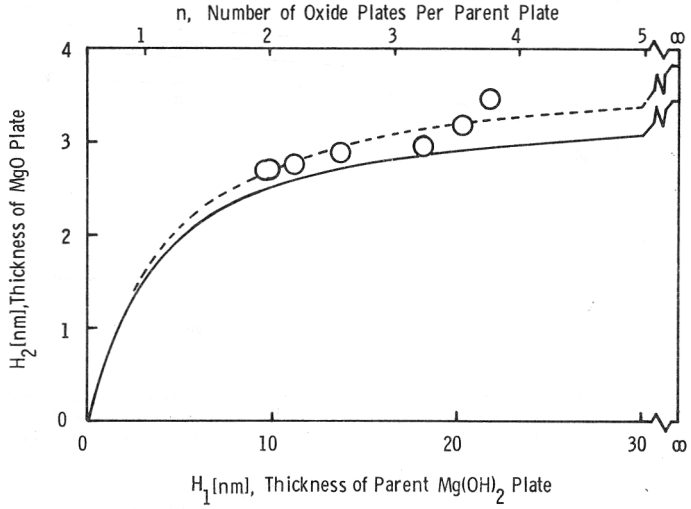

Figure 11. Relationship between parent and product plate thickness for the thermal decomposition of $Mg(OH)_2$ to MgO as calculated from Equation (13) (solid line). Circles are from Ref. (12), reducted by $\sqrt{3}$ (see text). Upper abscissa indicates the average number of MgO plates obtained from a parent ($Mg(OH)_2$. Broken line is calculated with a 10% reduction in the MgO density (see text).

also shown in Figure 11 reduced to the [111] dimensional thickness. Although the agreement with theory is reasonably good, a 10% reduction of the density of MgO to 3.22 g/cm³, broken line in Figure 11, greatly improves the results of Guilliat and Brett with theory. The hypothetical lower density is introduced due to the observation of a lower density (88%) in NiO[8,18], as noted earlier, and in CoO (75%)[19] which also could be considered as a member of the $M(OH)_2$/MO system[20]. Figure 12 is a similar plot for the $Ni(OH)_2$/NiO system indicating the difference between the two sample groups presented in Figure 9. The dotted lines represent the calculated results for NiO with the experimental density of 6.00 g/cm³ rather than 6.81 g/cm³ obtained from x-ray data. Both Figures 11 and 12 are labeled with two abscissae and two ordinates demonstrating the interrelationship of H_2 to n and H_1.

Interaction of Water with $Ni(OH)_2$

The 25 °C water adsorption isotherms for sample A and sample B are presented in Figure 13 in units of molecules adsorbed/nm². The following discussion is based upon the cross-sectional area of an H_2O molecule of 0.105 nm², representing a statistical monolayer of 9.52 molecules/nm². The B-point monolayers for sample A and sample B are 3.8 and 3.0 molecules/nm², respectively, indicating a relatively low polar site concentration on the surface. The degree of surface hydrophilicity of $Ni(OH)_2$ is apparently affected by the precipitation conditions used in its preparation.

The fact that the specific surface area of $Ni(OH)_2$ increases with decreasing concentration of $Ni(NO_3)_2$ is not surprising and can be explained by the expected

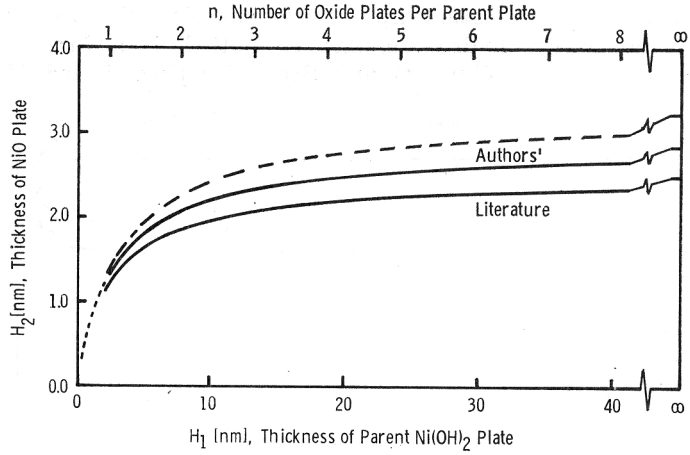

Figure 12. Relationship between parent and product plate thickness for the thermal decomposition of $Ni(OH)_2$ to NiO as calculated from Equation (13). Broken line calculated for authors' data with 12% reduction in NiO density (see text). Upper abscissa indicates the average number of NiO plates obtained from a parent $Ni(OH)_2$ plate for author's data.

decrease in the rate of growth of the crystallite particles. A change in the intrinsic surface properties of $Ni(OH)_2$ apparently as a function of the rate of crystal growth, however, is more difficult to explain.

It is possible to interpret the low water coverage from a different point of view involving crystallite size parameters or the relative microporosity of the two $Ni(OH)_2$ samples. The geometrical relationship between the specific surface area, Σ, of a regular hexagonal plate with radius or edge R, thickness H, and density ϱ, was previously expressed as:

$$\Sigma = \frac{2R + CH}{\varrho HR} \tag{1}$$

where

$$C = \frac{4\sqrt{3}}{3} = 2.309$$

Also, from the geometry of a single hexagonal plate, it can be shown that

$$\frac{\text{Edge Area}}{\text{Total Area}} = \frac{1}{1 + \frac{2R}{CH}} \tag{14}$$

If the plate radius is taken as 75 nm and specific surface area as 17 m^2/g, which are compatible with a typical $Ni(OH)_2$ plate of sample A, the value of H is calculated from Equation (1) as 52 nm. Equation (14) can then be used to show that the edge area is 44% of the total surface area. The monolayer coverage of 3.8 molecules/nm^2 found for sample A represents about 40% of total surface coverage. If the basal face planes of $Ni(OH)_2$ are hydrophobic and edge faces hydrophilic, monolayer coverage is proportional to the crystallite

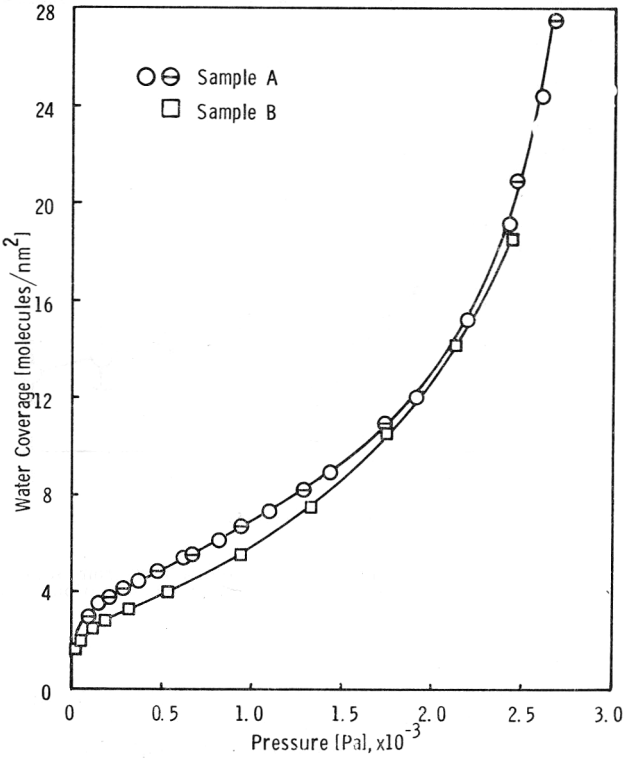

Figure 13. Water adsorption isotherms on two $Ni(OH)_2$ samples at 25 °C. One statistical monolayer would occur at 9.52 molecules/nm².

edge area. This might explain the difference in monolayer coverages between samples A and B as demonstrated in the adsorption isotherms in Figure 13 which are plotted as an intensive property independent of specific area. If the identical calculations are made for sample B, it is found that the crystallite thickness is 19.9 nm and the edge area represents 24% of the total surface area, whereas sample B actually shows about 32% hydrophilicity. These calculations are used only to demonstrate that edge area adsorption can possibly explain the degrees of surface hydrophilicity observed in Figure 13. This conclusion gains some support in recently published work on a fully hydroxylated ZnO $(10\bar{1}0)$ surface[21] which was found to have a low energy surface for water adsorption.

The multi-temperature water adsorption isotherms on sample A at 25° and 39 °C were used to calculate the isosteric heat of water adsorption as a function of coverage. The isosteric heat results, Figure 14, show that strong physical adsorption occurs at low coverages. The isosteric heat decreases from an initial value of 69 kJ/mole to 48 kJ/mole at coverage of 4 molecules/nm², then remaining essentially constant at higher coverages. The extent of strong physically adsorbed water should be compared with the B-point in each isotherm of sample A which occurs at 3.8 molecules/nm².

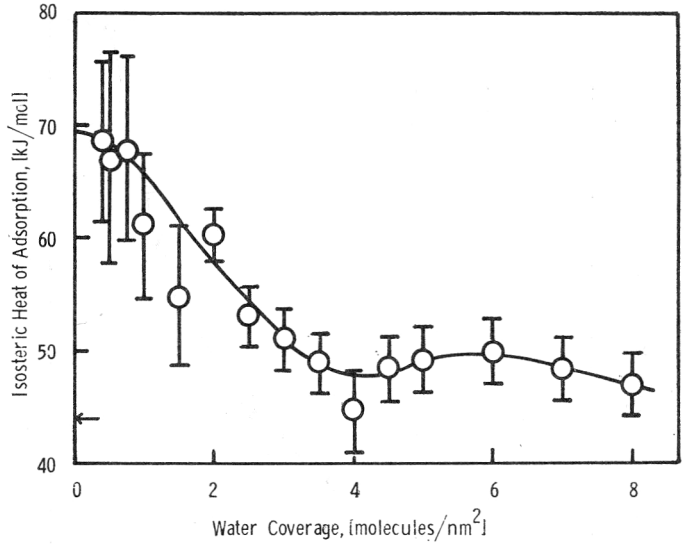

Figure 14. Isosteric heats of water adsorption were determined from multi-temperature isotherms on sample A. The arrow indicates the heat of condensation of water vapor.

Heats of Immersion in Water

The heat of immersion of sample A in water as a function of water precoverage was measured by means of an adiabatic calorimeter. The sample for each determination was first activated at 25 °C under a pressure of 10^{-6} mm for 24 hours and then allowed to equilibrate for one hour at a fixed water

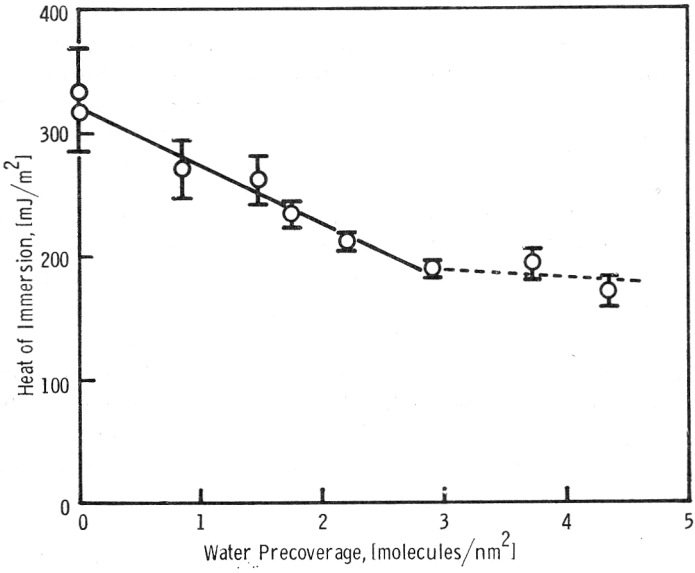

Figure 15. Heat of water immersion of sample A as a function of precoverage.

vapor pressure. The amount of water adsorbed under these conditions was determined from the 25 °C adsorption isotherm results in Figure 13. Zero water coverage in this context, therefore, means that the sample was not exposed to water vapor after undergoing the above activation conditions. The heats of immersion results for $Ni(OH)_2$ are given in Figure 15. The integral heat of immersion for the sample with zero precoverage is 320 mJ/m². The heat then decreases linearly with increasing coverage up to a water coverage of 3.0 molecules/nm², where a change in slope occurs with increasing water coverage.

The integral heat results in Figure 15 have been differentiated in order to determine the differential heat of adsorption. The calculated total differential heats are 72 kJ/mole and 47.9 kJ/mole in the water coverage ranges of 0—3.0 molecules/nm² and 3.0—5.0 molecules/nm², respectively. These results are in good agreement with the isosteric heats of adsorption.

Acknowledgements. The authors wish to thank S. Popović of the »Ruđer Bošković« Institute Zagreb, Croatia, Yugoslavia for the x-ray analysis and the National Science Foundation for its support of this work in a joint program with »Rudjer Bošković« Institute, Velimir Pravdić principal investigator.

REFERENCES

1. O. V. Krylov, *Kinet. Catal.* (English Edition), **3** (1962) 442.
2. C. M. Osburn and R. W. Vest, *J. Phys. Chem. Solids,* **32**, (1971) 1331; *J. Phys. Chem. Solids,* **32** (1971) 1343.
3. I. S. Shamina, *et al., Kinet. Catal. (English Edition),* **12** (1971) 603.
4. W. Huckel, *Structural Chemistry of Inorganic Compounds,* Vol. II, Elsevier Publishing Co., 1951, p. 547 ff.
5. N. H. Brett, K. J. D. MacKensie, and J. H. Sharp, *Q. Rev. (London),* **24** (1970) 185.
6. M. C. Ball and H. F. W. Taylor, *Mineralog, Mag.,* **32** (1961) 754.
7. J. F. Goodman, *Proc. Roy. Soc.* **A247** (1958) 346.
8. F. P. Larkins, P. J. Fensham, and J. V. Sanders, *Trans. Faraday Soc.,* **66** (1970) 1748.
9. J. V. Smith, (Ed.), *X-ray Powder Data File,* ASTM, Philadelphia, (1967).
10. N. Bonacci and D. M. Novak, *Croat. Chem. Acta,* **45** (1973) 531.
11. A. C. Zettlemoyer and W. C. Walker, *Ind. Eng. Chem.,* **39** (1947) 69.
12. I. F. Guilliatt and N. H. Brett, *Phil. Mag.,* **23** (1971) 647.
13. I. F. Guilliatt and N. H. Brett, *Phil. Mag.,* **21** (1970) 671.
14. S. J. Teichner and J. A. Morrison, *Trans. Faraday Soc.,* **51** (1955) 961.
15. K. Klier, *Kinet. Catal. (English Edition),* **3** (1962) 51.
16. R. S. Gordon and W. D. Kingery, *J. Amer. Ceram. Soc.,* **50** (1967) 8.
17. P. J. Anderson and R. F. Horlock, *Trans. Faraday Soc.,* **58** (1962) 1993.
18. W. R. Helms and J. G. Mullen, *Phys. Rev. B.,* **4** (1971) 750.
19. H. N. Ok and J. G. Mullen, *Phys, Rev.,* **168** (1968) 550; Erratum: *Ibid.,* **181** (1969) 986.
20. I. F. Hazell and R. J. Irving, *J. Chem. Soc. (London), A,* (1966) 669.
21. T. Morimoto and M. Nagao, *J. Phys. Chem.,* **78** (1974) 1116.
22. G. A. Nicolaon and S. J. Teichner, *J. Coll. Interface Sci.,* **38** (1972) 172.
23. A. Merlin and S. Teichner, *Compt. rend.,* **236** (1953) 1892.
24. J. D. Cotton and P. J. Fensham, *Trans. Faraday Soc.,* **59** (1963) 1444.
25. P. C. Gravelle and S. J. Teichner, *Adv. in Catal.,* **20** (1969) 167.
26. O. V. Krylov and Z. A. Markova, *Kinet. Catal.* (English Ed.), **6** (1965) 107.
27. R. I. Razouk and R. S. Mikhail, *J. Phys. Chem.,* **63** (1959) 1050.

SAŽETAK

Karakterizacija $Ni(OH)_2$ i NiO velike površine

C. Cronan, F. J. Micale, H. Leidheiser, Jr., M. Topić i A. C. Zettlemoyer

Rad prikazuje rezultate dobivene različitim eksperimentalnim tehnikama o površinskim svojstvima $Ni(OH)_2$ i NiO te mehanizam prelaza $Ni(OH)_2$ u NiO. Nikal-hidroksid dobiven je taloženjem amonijakom otopine nikal-nitrata. Nikal-oksid velike površine dobiven je dehidratacijom $Ni(OH)_2$ kod povišene temperature.

Veza između specifične površine početnog $Ni(OH)_2$ i produkta NiO ukazuje na mehanizam dehidratacije kod 200 °C koji uključuje separaciju duž heksagonalnih ravnina. Mehanizam je potvrđen snimkama elektronskim mikroskopom tokom dekompozicije.

Gravimetrijska analiza razlaganja $Ni(OH)_2$ pri 200 °C i mjerenje reflektiranih i. r.-spektara pokazali su da se ne mogu s površine ukloniti sve hidroksilne skupine. Fizikalna adsorpcija vodene pare na $Ni(OH)_2$ kao funkcija specifične površine podržava hipotezu da su osnovne ravnine hidrofobne, a kristalni kutovi hidrofilni.

CENTER FOR SURFACE AND COATINGS RESEARCH
LEHIGH UNIVERSITY,
BETLEHEM, PA., USA